https://doi.org/10.5194/egusphere-2026-1060
Preprint. Discussion started: 24 June 2026

Range-resolved retrieval of aerosol particle size distribution during Saharan dust intrusions over the Bavarian Alps using multiwavelength lidar observations.

Michal A. Posyniak[1], Stefan Sitarek[2], Johannes Speidel[1], Tadeusz Stacewicz[2], Hannes Vogelmann[1]

[1]Institute of Meteorology and Climate Research - Atmospheric Environmental Research, Karlsruhe Institute of Technology, Garmisch-Partenkirchen, 82467, Germany
[2]Institute of Experimental Physics, Faculty of Physics, University of Warsaw, 02-093 Warsaw, Poland

Correspondence to: Michal A. Posyniak (michal.posyniak@kit.edu)

Abstract. We present ground-based remote sensing observations of Saharan dust over the Bavarian Alps during three events on 29 February, 29 March, and 29 April 2024, with emphasis on aerosol particle size distribution (APSD) retrieval from multiwavelength lidar measurements. Raman–depolarization lidar observations from Garmisch-Partenkirchen were combined with sun-photometer data from the summit of Zugspitze. Long-range transport from North Africa was confirmed using back-trajectory analysis and aerosol forecasts. Elevated dust layers extending up to 6–7 km a.s.l. were observed, frequently structured into multiple layers.

APSDs were retrieved by applying an inversion method that directly substitutes predefined (bi-modal log-normal) size distributions into the lidar equations, reducing the inversion to the estimation of a limited set of microphysical parameters. This approach enables range-resolved retrievals of effective particle radius, yielding values up to 3–4 µm within dust layers and decreasing with altitude. Comparison with column-integrated sun-photometer retrievals shows consistent coarse-mode effective radii (1.2–1.4 µm). The results highlight both the strengths and limitations of APSD retrieval from lidar, particularly regarding assumptions on particle shape and refractive index.

1 Introduction

Aerosol particles significantly influence both the climate system and air quality. Their impact on climate can manifest in either a warming or cooling effect, contingent upon their distinctive physical and chemical attributes and their capacity to alter the reflectance of the Earth's surface. Hence, the interplay between aerosols and climate can yield disparate outcomes on a regional scale compared to the global context. Moreover, the regional ramifications of aerosols on climate and weather tend to surpass their global average effects, due to their relatively brief atmospheric persistence and the non-uniformity in their sources, dispersion, and deposition patterns. Aerosols can also significantly affect the climate on the regional scale, primarily due to heightened concentrations of particles and their interaction with specific weather conditions and local topography. Therefore, it's important to recognize the critical role of long-range transport in the dynamics of aerosol distribution. The transport of

https://doi.org/10.5194/egusphere-2026-1060
Preprint. Discussion started: 24 June 2026

aerosols over extensive distances can substantially affect their dispersion patterns, introducing complexities in both regional climate dynamics and air quality regulation. (Carslaw et al., 2010, Seinfeld et al., 2016, Zhang, B., 2020)

Deserts are the primary global source of mineral aerosols, most importantly the Sahara. It is estimated that each year, several hundred million to billions of tons of desert dust from the Sahara are transported over the tropical regions of the Atlantic Ocean and the Mediterranean Sea (Balis et al., 2004). The particles of desert aerosol are nonspherical, and their shape and size distribution are strongly influenced by wind speed (Seinfeld and Pandis, 1997). Higher wind speeds facilitate the suspension of larger particles into the atmosphere. Generally, three modes of particle size distribution can be distinguished by radius: 0.005 µm or less, approximately 0.02 µm, and 5 µm. During desert storms, dust is frequently lifted into the upper tropospheric layers. The smallest particles ($r < 5$ µm) can remain in the atmosphere for up to two weeks and can be transported over distances of several thousand kilometers. However, very large particles with radii larger than 50 µm do not extend beyond the source regions (Seinfeld and Pandis, 1997).

In this study, we investigate the optical properties of mineral dust transported in the middle troposphere from the Sahara Desert to the Bavarian Alps. The analysis is based on lidar observations performed during distinct dust episodes in February, March, and April 2024. These Saharan dust plumes were advected by persistent southerly flows and transported over central Europe, reaching sites such as Garmisch-Partenkirchen (47°N, 11°E). Such events are common in springtime and have been extensively reported (Papayannis et al., 2008; Papanikolaou et al., 2024). While numerous studies exist on Saharan dust in southern Europe (e.g., Balis et al., 2004; Papayannis et al., 2005; Mylonaki et al., 2021), reports from Central and Northern Europe remain relatively scarce (e.g., Ansmann et al., 2003; Papanikolaou et al., 2024). Systematic observations of desert dust using lidar have been conducted in the Zugspitze area since the 1980s (Jäger et al., 1988). Lidar observations from Garmisch-Partenkirchen revealed elevated aerosol layers indicative of desert dust transport and stratosphere-to-troposphere intrusion over the northern Alps (Trickl et al., 2020). Therefore, detailed characterization of desert aerosol properties at higher latitudes continues to be of high scientific interest.

The observations presented here contribute to the broader goals of the Aerosol, Clouds and Trace Gases Research Infrastructure (ACTRIS), which aims to provide long-term, high-quality atmospheric profiling across Europe. Our measurements were performed within the framework of the European Aerosol Research Lidar Network (EARLINET, Pappalardo et al., 2014), a key component of ACTRIS, which has been operational since 2000. Garmisch-Partenkirchen has a long and established tradition in lidar-based aerosol remote sensing and has been an active EARLINET site from the very beginning (Pappalardo et al., 2008). The site has played a central role in advancing ground-based aerosol profiling in Europe and remains a cornerstone for harmonized observations and intercomparisons (Sicard et al., 2015).

To enhance our understanding of aerosol optical and microphysical properties (Liu et al., 2014), researchers have utilized both remote sensing techniques and in situ methods through various atmospheric probing platforms (Devara, 1998). Ground-based remote sensing techniques rely on instruments like sun photometers and lidars. Sun photometers facilitate the determination of columnar aerosol properties, including aerosol optical depth (AOD) and single scattering albedo, while lidars offer vertical profiles of aerosol optical properties, such as backscatter and extinction coefficients (Speidel and Vogelmann, 2023), as well

https://doi.org/10.5194/egusphere-2026-1060
Preprint. Discussion started: 24 June 2026

as depolarization ratio. From the latter, information about the particle shape (spherical/nonspherical) can be concluded. Lidar measurements provide data with high temporal resolution, typically in the range of seconds to minutes, and a spatial resolution of the order of 10 meters.

Optical remote sensing of aerosols is one of the essential methods when it comes to the investigation of aerosol concentrations and their composition. Photometers and lidars, working simultaneously at several wavelengths, are nowadays widely used for such observations. Active remote sensing using lidar technology serves as a crucial method for studying atmospheric aerosols (Mylonaki et al., 2024). The particle backscatter coefficient at a single wavelength is commonly retrieved with the Klett inversion algorithm (Klett, 1985), improved by Speidel and Vogelmann (2023). In contrast, the capabilities offered by multiwavelength lidars (e.g., $3\beta+2\alpha+2\delta$) are particularly advantageous, as they allow for the determination of range-resolved Aerosol Particle Size Distribution (APSD). This function is essential for assessing aerosol optical properties. The simultaneous operation of a photometer and a lidar, located side by side or close to each other, provides the opportunity to retrieve vertical profiles of optical and microphysical properties of aerosol from almost the same air volume.

Böckmann (2001) introduces a specialized method for retrieving aerosol particle volume distribution, mean refractive index, and other critical physical parameters from multiwavelength lidar measurements. This technique addresses the challenges associated with the ill-posed nature of inverting lidar data, enhancing the accuracy and reliability of aerosol characterization. The methodological advancement in lidar aerosol retrieval, demonstrating that the use of longer (over 1064 nm) infrared wavelengths improves the detection and characterization of coarse aerosol modes, was presented in Böckmann (2024).

Software like Generalized Retrieval of Aerosol and Surface Properties (GRASP, Dubovik et al., 2021) allows for providing not only the detailed retrieval of columnar aerosol properties but also the information about aerosol vertical distribution. The synergy of radiometer and lidar data provides information that is not available if only radiometer or lidar data were used. This software allows for the retrieval of concentration profiles of fine and coarse modes of aerosol particles. (Lopatin et al., 2021). In this paper, we will present the application of an APSD retrieval by a software for retrieving the effective radius of aerosol particles from multiwavelength lidar returns (Jagodnicka et al, 2009; Sitarek et al., 2016). In this method, a predefined APSD function with a few free parameters is directly substituted into the lidar equations. While this software was originally developed for aerosol observation under cumulus clouds (Stacewicz et al., 2014) and studies of aerosol over the Baltic Sea (Makuch et al., 2021), we now apply it for the characterization of mineral dust outbreaks from the Sahara, reaching Central Europe after being transported over longer distances, which came along with a certain ageing of the aerosol load.

2 Mineral dust events

In the first half of 2024, intensive Saharan dust events occurred over Western Europe. Observations in Garmisch-Partenkirchen were possible during several days from February to June. In this paper, the authors will focus only on three cases from 29 February, 29 March, and 29 April 2024. These days (except 29 March) were selected due to clear-sky conditions, which allowed parallel lidar and sun photometric measurements. The choice of 29 March was driven by an unusually intense influx

https://doi.org/10.5194/egusphere-2026-1060
Preprint. Discussion started: 24 June 2026

of desert dust. Despite the cloud cover and the lack of photometric data, it was decided to include this day in the analysis as well.

On 29 February 2024, the Azores high ridge merged with a high-pressure system over Russia, separating the prevailing low-pressure system over the northern Atlantic from the Mediterranean low. The backward trajectories of the air masses from HYSPLIT (Stein et al., 2015) indicate that a warm air mass from North Africa was transported over Germany to the observation region (Fig 1a) following a direct cyclonic path. This resulted in a high dust load, which was also predicted as AOD calculated with the ICAP-MME (in Fig. 2a, International Cooperative for Aerosol Prediction) model (Xian et al., 2019).

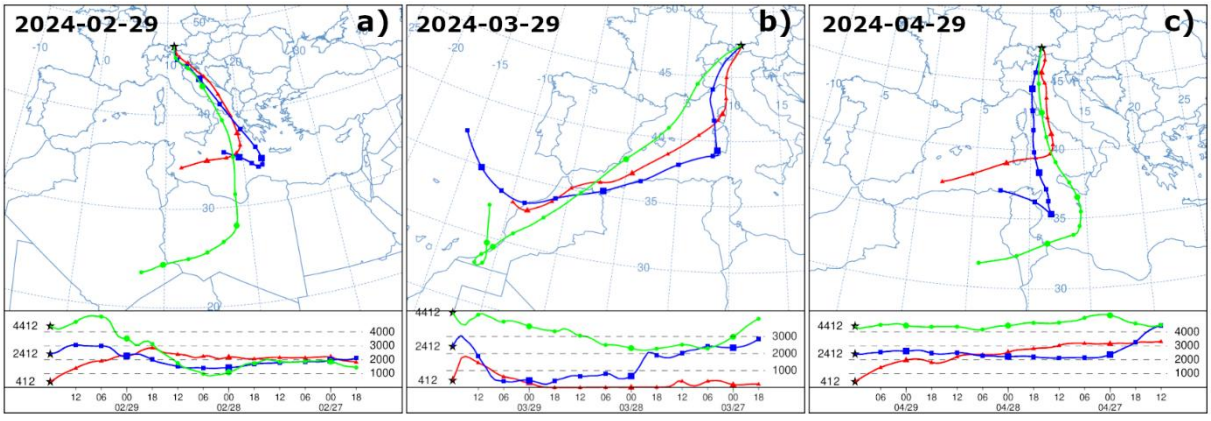

Figure 1: HYSPLIT back-trajectories obtained for Garmisch-Partenkirchen for (a) 29 February 2024, (b) 29 March 2024, and (c) 29 April 2024. The HYSPLIT model was run for 72 h with meteorological data from the Global Data Assimilation System (GDAS). Trajectories altitude is shown in meters above ground level (in the model), which corresponds to 2000, 4000, and 6000 m above sea level.

In the second case (29 March 2024), the weather in Western Europe was shaped by a low-pressure system centered around Ireland and central England, as well as a high-pressure system centered over Libya. A warm front was moving north from northern Italy, bringing high-level cloud cover. Air from the Morocco region was directly flowing over the Alps into southern Germany (Fig. 1b). Along with this pronounced fast airstream, a rapid transport of desert dust was predicted by ICAP-MME (Fig. 2b). The trajectory ending at ~4000 m indicates that the air masses travelled approximately 1300 km in 18 hours, over twice the speed seen in the other two cases.

On April 29, 2024, a high-pressure system with two centers, one over northern Russia and another over eastern Belarus, was present. In Western Europe, a large multi-centered low-pressure system was situated over the British Isles and the Faroe Islands. A shallow trough of low pressure over the Alps with an undulating cold front associated with this system extended from Scandinavia through the Danish Straits, Germany, and down to the Mediterranean Sea, slightly brushing the southern edges of Germany. This synoptic situation resulted in Saharan dust advection on a rather direct path (Fig. 1c and Fig. 2c).

https://doi.org/10.5194/egusphere-2026-1060
Preprint. Discussion started: 24 June 2026

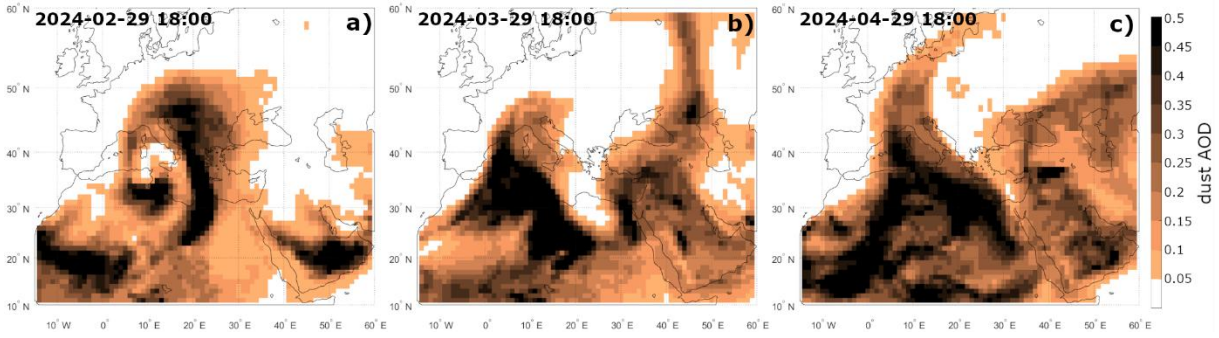

Figure 2: Forecast of AOD of the dust component from the ICAP-MME model for (a) 29 February 2024, (b) 29 March 2024, and (c) 29 April 2024 (in all cases for 18 UTC).

In all cases, the dominant aerosol fraction was mineral dust. Figure 3 presents time-dependent profiles of dust mixing ratios from the CAMS model (Inness et al., 2019) to show that the dust was partially uplifted far into the free troposphere in all three cases. The concentration of dust particles of sizes from 0.9 to 20 µm on 29 February 2024 reaches values about 0.3-1 10-4g/kg, and the layer starts at the surface and reaches an altitude of 6 km. On 29 March 2024, we observed a layer of dust starting at 2 km and growing with time to ~6 km. The maximum mixing ratio of dust was prognosed as ~2 10-4g/kg. On 29 April 2024, the concentration was reaching 3.7 10-4 g/kg, and the maximum altitude of the layer was less than 6 km.

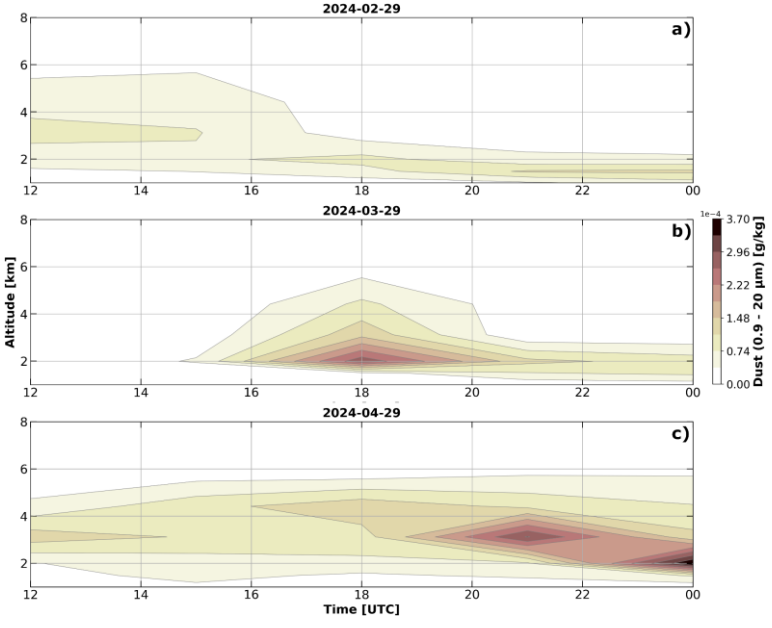

Figure 3: Forecast of dust particles (sizes from 0.9 to 20 µm) from the CAMS model for (left) 29 February 2024, (center) 29 March 2024, and (right) 29 April 2024.

https://doi.org/10.5194/egusphere-2026-1060
Preprint. Discussion started: 24 June 2026

Saharan dust advection led to notably reduced visibility. This can be observed in the photographs taken on 29 February, 29 March, and 29 April 2024 (Fig. 4 a, b, and c) from the summit of Zugspitze looking south. These images are compared with a photograph taken under very good visibility conditions (Fig. 4 d).

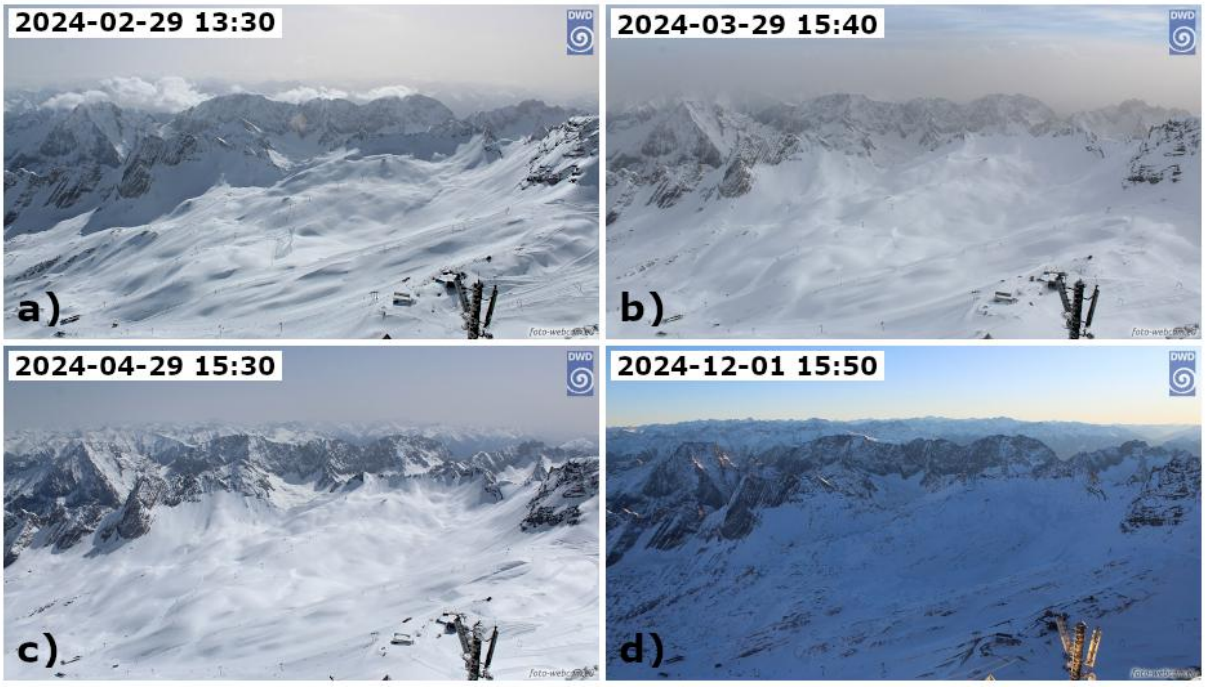

Figure 4: Photographs taken on (a) 29 February 2024 (13:30 CET), (b) 29 March 2024 (15:40 CET), and (c) 29 April 2024 (15:30 CET) from the summit of Zugspitze looking south. These images are compared with a photograph taken under good visibility conditions (d) on 1 December 2024 (15:50 CET). Image source: www.foto-webcam.eu.

2 Instrumentation and data processing technique

2.1 Equipment

The remote sensing equipment is located in the valley of Garmisch-Partenkirchen (734 m a.s.l.) at Karlsruhe Institute of Technology (KIT) Campus Alpin and on the top of Mount Zugspitze (2962 m a.s.l.). The horizontal distance between the two sites is approximately 7 km. This infrastructure belongs to ACTRIS-D national facilities (Laj et al., 2024)

The Cimel CE318-T sun/sky/lunar photometer is installed at the summit of Mount Zugspitze. This atmospheric observation facility is a part of the AERONET network (Giles et al., 2015) and can be seen as representative of the atmospheric conditions at high altitudes over central Europe. It is assumed that the top of Zugspitze is usually above the planetary boundary layer (PBL) during most of the year, but certainly during the winter season. On the other hand, in summer, the PBL occasionally reaches up to 4 km a.g.l. (e.g., Vogelmann et al., 2015), So it is over 2/3 of its height. This renders Zugspitze a suitable site for

https://doi.org/10.5194/egusphere-2026-1060
Preprint. Discussion started: 24 June 2026

observing long-range transport of aerosol layers in the free troposphere, because measurements are not affected by ground emissions and low-level advection.

The lidar station located in Garmisch-Partenkirchen is a part of EARLINET. However, after 2015, aerosol measurements with lidar were only operated at Schneefernerhaus on Zugspitze (Trickl et al., 2024). At the beginning of 2024, the aerosol lidar "TONI", as part of ACTRIS, was implemented at KIT Campus Alpin. The lidar system manufactured by Raymetrics is based on a diode-pumped Nd: YAG laser, transmitting 3 wavelengths: 1064, 532, and 355 nm. Energies of light pulses are 90, 90, and 50 mJ, respectively, while the repetition rate is 100 Hz. The lidar receiver is equipped with seven detection channels, including three for measuring elastic backscatter (β), two for Raman signals used to retrieve aerosol extinction profiles (α), and two depolarization channels (δ) designed to assess particle nonsphericity and infer aerosol type. The usage of a 300 mm diameter mirror together with an off-axis laser beam geometry results in a full overlap near 250 m, making this device suitable for observations of aerosols in the Planetary Boundary Layer (PBL) and the free troposphere.

2.2 Software description

In order to retrieve APSD from multiwavelength lidar signals, the software described in Sitarek et al. (2016) was applied. APSD Software is a stand-alone desktop application designed for the retrieval of aerosol particle size distributions from multiwavelength lidar measurements. The software is based on a direct-fitting approach, in which synthetic lidar signals generated from an assumed aerosol particle size distribution are compared with experimentally measured lidar returns. The optimal aerosol parameters are determined through minimization of a cost function describing the difference between modeled and measured signals.

Before the inversion, the user specifies the wavelengths of the analyzed lidar channels, the particle radius range used in Mie calculations, and the complex refractive index of the investigated aerosol. The refractive index can be selected from predefined aerosol types or supplied as an external wavelength-dependent file. Measured lidar signals are provided in ASCII format, with the first column containing altitude and subsequent columns containing signals corresponding to individual wavelengths. The software can process both raw and range-corrected lidar signals. For raw measurements, several pre-processing options are available, including signal sign correction, offset removal, smoothing, and generation of range-corrected signals.

The retrieval is constrained to a predefined bimodal lognormal aerosol model. The number of modes and their widths are fixed a priori, while the modal radii and concentrations are optimized during the inversion procedure. As a result, the retrieved APSD represents the best-fitting bimodal approximation of the observed aerosol population. The software provides altitude-resolved aerosol particle size distributions together with profiles of effective radius calculated from the retrieved APSD.

2.2.1 Method for the APSD retrieval

In this approach, it is assumed that the backscattering lidar provides distance (z) dependent range corrected signals $L_1(z)$, $L_2(z)$, …, $L_\Lambda(z)$ corresponding to various wavelengths ($\lambda = 1, 2, \ldots \lambda$). The following set of equations can represent these signals:

https://doi.org/10.5194/egusphere-2026-1060
Preprint. Discussion started: 24 June 2026

$$L_\lambda(z) = A_\lambda \beta_\lambda(z) exp\left(-2\int_{z_0}^{z} \alpha_\lambda(y)dy\right), \quad (1)$$

where z_0 corresponds to lidar position, A_λ are the wavelength-dependent apparatus constants, while $\alpha_\lambda(z)$ and $\beta_\lambda(z)$denote the spatial distributions of total atmospheric extinction and backscattering coefficients, respectively. Each distribution can be expressed as a sum of constituents (Seinfeld and Pandis, 1997):

$$\alpha_\lambda(z) = \alpha_{R\lambda}(z) + \alpha_{A\lambda}(z) = \alpha_{R\lambda}(z) + \int_0^\infty Q_\lambda^E(r)\pi r^2 n(z,r)dr, \quad (2)$$

$$\beta_\lambda(z) = \beta_{R\lambda}(z) + \beta_{A\lambda}(z) = \beta_{R\lambda}(z) + \int_0^\infty Q_\lambda^B(r)\pi r^2 n(z,r)dr. \quad (3)$$

The first constituents of (2) or (3) correspond to Rayleigh scattering. For a standard atmosphere, $\alpha_{R\lambda}(z)$ and $\beta_{R\lambda}(z)$ can be evaluated using the approach of Bodhaine et al. (1999). Second constituents in Eq. (2) and (3), *i. e.*, $\alpha_{A\lambda}(z)$ and $\beta_{A\lambda}(z)$, correspond to aerosol scattering. The aerosol is assumed to consist of spherical particles of known refractive index. Then $\alpha_{A\lambda}(z)$ and $\beta_{A\lambda}(z)$ are described by relevant integrals. Function $n(z,r)$ is the distance-dependent aerosol particle size distribution (APSD). Here r describes the particle radius, while Q_λ^E(r) and Q_λ^B(r) are the extinction and backscattering efficiencies, respectively. Both were evaluated using Mie theory (Bohren and Huffman, 1999).

The presented approach consists of the direct substitution of α_λ and β_λ coefficients in form (2, 3) into equations (1). As a result, only one unknown function remains: the APSD, which is the matter of investigation.

In this approach, the APSD was assumed in a predefined form of a log-normal function:

$$n_j(z,r) = \frac{C_j(z)}{\sqrt{2\pi}\cdot log\sigma_j(z)} \cdot \frac{1}{r} \cdot exp\left\{\frac{-[logr - logR_j(z)]^2}{2\cdot log^2\sigma_j(z)}\right\}, \quad (4)$$

or a linear combination of log-normal modes:

$$n(z,r) = \sum_{j=1}^{K} n_j(z,r). \quad (5)$$

Here, R_j denotes the modal radius, C_j – the concentration of aerosol in a given mode, and σ_j – the mode width. Then the inversion reduces to determining the optimal parameters of these modes.

The lidar returns, which are provided by the apparatus, are quantified in space with the interval Δz resulting from the digitization rate and smoothing procedure. At a distance z_l for each wavelength, the signals can be expressed by:

$$L_\lambda(z_l) = A_\lambda \beta_\lambda(z_l) exp\{-\Delta z \sum_{i=2}^{l}[\alpha_\lambda(z_{i-1}) + \alpha_\lambda(z_i)]\}. \quad (6)$$

The integral from Eq. (1) was approximated by use of the trapezoidal approach. For further analysis, the ratio of the signals at distances z_l and $z_{l+1} = z_l + \Delta z$ is taken:

$$\frac{L_\lambda(z_{l+1})}{L_\lambda(z_l)} = \frac{\beta_\lambda(z_{l+1})}{\beta_\lambda(z_l)} exp\{-\Delta z[\alpha_\lambda(z_l) + \alpha_\lambda(z_{l+1})]\}. \quad (7)$$

This allows the omission of the apparatus constants A_λ, which are usually unknown, and of the lidar ratio.

The left-hand side of formula (7) describes the ratio of the experimental signals, while the extinction and backscattering coefficients in formulas (2) and (3) are substituted for the right side of the equations. Since both coefficients depend on the aerosol distribution in equation (7), only one unknown function (i.e., APSD) remains. Therefore:

$$\frac{L_\lambda(z_{l+1})}{L_\lambda(z_l)} = \frac{\int_0^\infty r^2 Q_\lambda^B(r) n(z_{l+1},r)dr}{\int_0^\infty r^2 Q_\lambda^B(r) n(z_l,r)dr} exp\left\{-\Delta z\left[\int_0^\infty \pi r^2 Q_\lambda^E(r) n(z_l,r)dr + \int_0^\infty \pi r^2 Q_\lambda^E(r) n(z_{l+1},r)dr\right]\right\}. \quad (8)$$

https://doi.org/10.5194/egusphere-2026-1060
Preprint. Discussion started: 24 June 2026

The distribution $n(z, r)$ in a predefined form of a two-mode lognormal function (5) with several free parameters $\{C_1, R_1, \sigma_1, C_2, R_2, \sigma_2\}$ is used in our approach. The solution of Eq. (8) is performed with a minimization technique. For this purpose, we construct a cost function based on Eq. (8):

$$\chi^2(z_l) = \sum_{\lambda=1}^{\Lambda} \left(\frac{L_\lambda(z_{l+1})}{L_\lambda(z_l)} - \frac{\beta_\lambda(z_{l+1})}{\beta_\lambda(z_l)} exp\{-\Delta z[\alpha_\lambda(z_l) + \alpha_\lambda(z_{l+1})]\} \right)^2. \quad (9)$$

The function $n^{min}(r,z)$ with the set of parameters that corresponded to the minimal value of the cost function (9) should be accepted as the solution. However, the bimodal lognormal function found by such a minimization procedure is not unique. Quite satisfactory results (i.e., the comparable values of χ^2 parameter) were achieved for several different $\{C_1, R_1, \sigma_1, C_2, R_2, \sigma_2\}$ sets. Therefore, a group of 300 of the results with the smallest χ^2 was chosen. The values of χ_i^2 (i = 1 ÷ 300) for each set of such parameters did not differ by more than about several tens of percent.

Bimodal lognormal function n_i^{min} was generated for each set of such parameters. As a final result of APSD retrieval, the weighted average of these functions was accepted.

$$n_{opt}(r,z) = \frac{\sum_{i=1}^{300} \chi_i^{-2} n_i^{min}}{\sum_{i=1}^{300} \chi_i^{-2}} \quad (10)$$

The values of χ_i^{-2} were taken as weights for this averaging.

Finally, such APSD function was used for the calculation of the effective radius (r_{eff}) of aerosol particles by means of the formula:

$$r_{eff}(z) = \frac{\int_0^\infty r^3 n_{opt}(r,z) dr}{\int_0^\infty r^2 n_{opt}(r,z) dr}. \quad (11)$$

As mentioned above, in our work, we assume that the aerosol particles are spherical. It is well known that in reality their shape is highly irregular, especially the desert dust particles. Some authors (Hoshiarpur et al., 2019; Huang et al., 2023) try to improve the agreement of theoretical models with measurement results by assuming an ellipsoidal shape of particles with different parameters. The non-sphericity of the particles leads to strong depolarization of the scattered light. Volume depolarization measurements were available and were used for aerosol typing. However, particle depolarization ratios required for quantitative correction of particle nonsphericity in the APSD retrieval were not available. We cannot state whether such an approach would lead to a better interpretation of our results. For example, the analysis carried out by Bi *et al.* (2019) for ellipsoidal salt particles with different degrees of hydration - and therefore different degrees of asymmetry - did not show differences greater than 20% in the radiation scattering efficiencies.

3 Results

3.1 Characterization of Saharan Dust Events

Curtain plot of the dust event from 29 February 2024 is shown in Fig. 5 a. On that day, multiple dust layers reaching up to 7 km a.s.l. were observed. The first layer extends from 3 to 3.5 km a.s.l. The second layer, containing sublayers, is present above

https://doi.org/10.5194/egusphere-2026-1060
Preprint. Discussion started: 24 June 2026

~4 km. On 29 March 2024, the dust layer was present up to 4 km (Fig. 5 b). During Saharan dust advection on 29 April 2024, two layers of dust were also present. The lower layer reached up to approximately 2 km, later decreasing its height to 1km. The second layer was present between 3 and 5 km. Until 13:05 UTC, over the Garmisch lidar site, clouds were present (Fig. 5 c).

The enhanced values of volume depolarization ratio observed within the identified layers (Fig. 5 d-f) indicate the presence of non-spherical particles and are consistent with the expected depolarization signature of Saharan dust reported in previous lidar studies (e.g., Freudenthaler et al., 2009; Tesche et al., 2009; Groß et al., 2011).

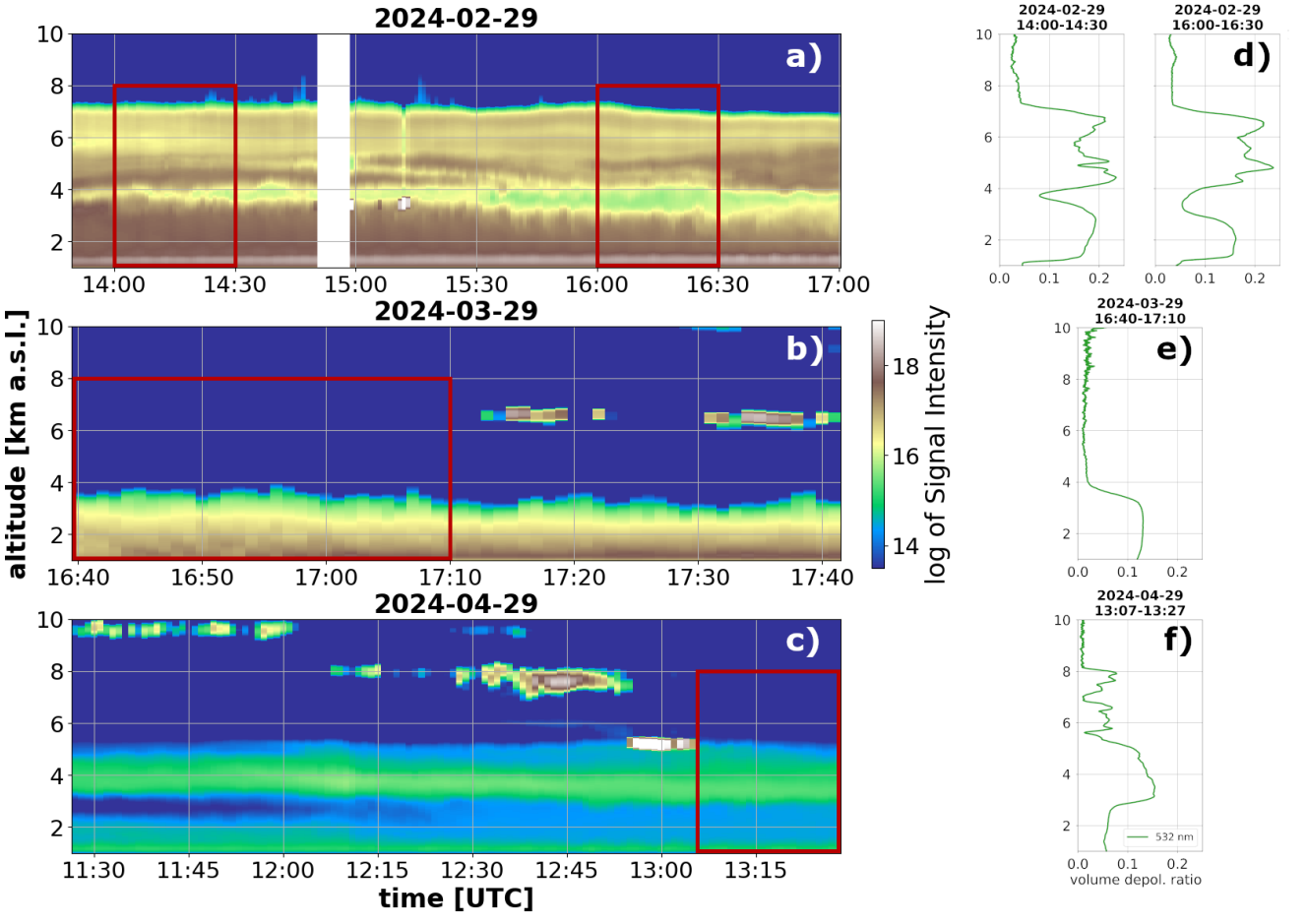

Figure 5: Curtain plots of the logarithm of the range-corrected signal at 1064 nm measured with the TONI lidar on (a) 29 February 2024, (b) 29 March 2024, and (c) 29 April 2024. The regions highlighted by red rectangles indicate the signal intervals selected for further analysis. The panel on the **right-hand side shows the mean volume depolarization ratio (at 532 nm) profiles corresponding to the selected periods.**

The evolution of the changes of AOD at 500 nm and an Ångstrom exponent (AE) of 440-870 nm measured on Zugspitze during the measurement days is presented in Fig. 6. On 29 February 2024, values of AOD were decreasing from ~0.2 at noon

https://doi.org/10.5194/egusphere-2026-1060
Preprint. Discussion started: 24 June 2026

to ~0.1 in the afternoon. The higher AOD values were related to dust advection, which is clearly visible on the AE plot. The values of AE are getting smaller with the growth of AOD, which corresponds to the presence of big particles - dust. On 29 April 2024, we observed growth of AOD during the day, but in this case, the values were almost twice as high and varied from ~0.15 to ~0.25, and the AE values were higher than in February. This indicates the presence of smaller particles than on 29 February around noon, but still, AE values indicated the presence of large particles. It is worth mentioning that on 29 March 2024, there were no photometric measurements due to cloud cover.

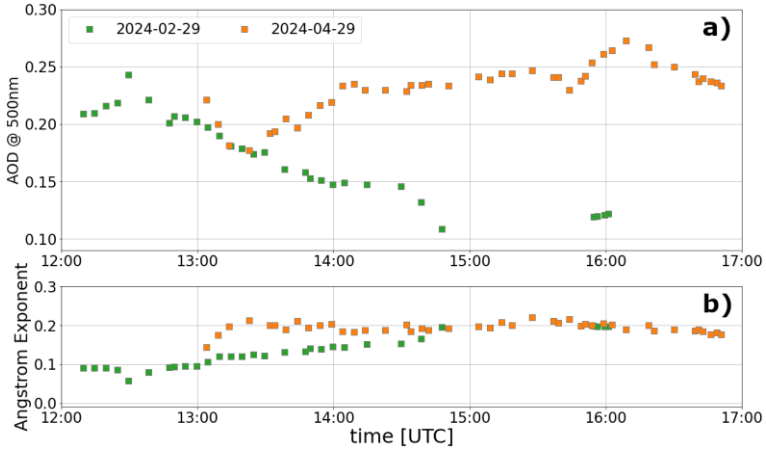

Figure 6: Diurnal changes of a) aerosol optical depth at 500 nm and b) 440-870 Angstrom exponent measured at Zugspitze on 29 February 2024 (green) and 29 April 2024 (orange).

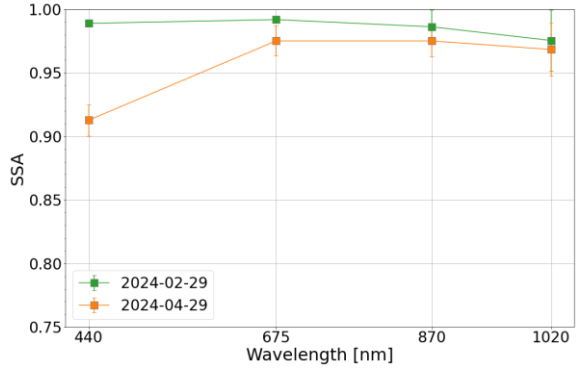

Figure 7: Mean values of single scattering retrieved from photometric measurements at Zugspitze on 29 February 2024 (green) and 29 April 2024 (orange).

Single scattering albedo (SSA) retrieved from photometric measurements at Zugspitze (Fig. 7) shows that the aerosol present in the layers is likely to be mineral dust (Shin et al., 2019), especially on 29 April 2024. On the other hand, SSA on 29 February 2024 points out that it is a mixture of anthropogenic and dust aerosol (Shin et al., 2019).

https://doi.org/10.5194/egusphere-2026-1060
Preprint. Discussion started: 24 June 2026

3.2 Effective radius of dust particles

Three cases were chosen for r_{eff} retrieval. For the first and second cases, two signals from 29 February 2024 registered between 14:00 and 14:30 and between 16:00 and 16:30 were selected. For the third case, the measurements from 29 April 2024 taken between 13:07 and 13:27 (when the measurements ended) were chosen. When selecting windows for the analysis, the primary selection criterion was the absence of cloud cover, as it significantly affects signal retrieval.

To determine the aerosol properties, mean lidar profiles were calculated for cloudless conditions. The profiles were also spatially averaged over 150 m thick layers. For the effective radius retrieval, the analysis used an average value of the refractive index derived from AERONET measurements, approximately 1.46 at 532 nm.

To obtain those profiles, lidar signals had to be prepared first. APSD software is designed to operate on so-called "total" signals. In the case of our lidar at wavelengths 355 and 532 nm, we have parallel and cross-polarized channels. Thus, to obtain the total signal, the returns from cross and parallel polarization channels were summed up. The method by Freudenthaler (2016) was used for this purpose. Moreover, the Automated Lidar Quality Analysis Software (ATLAS, Freudenthaler et al., 2018) software was used for the calculation of gain ratios and the crosstalk between the channels.

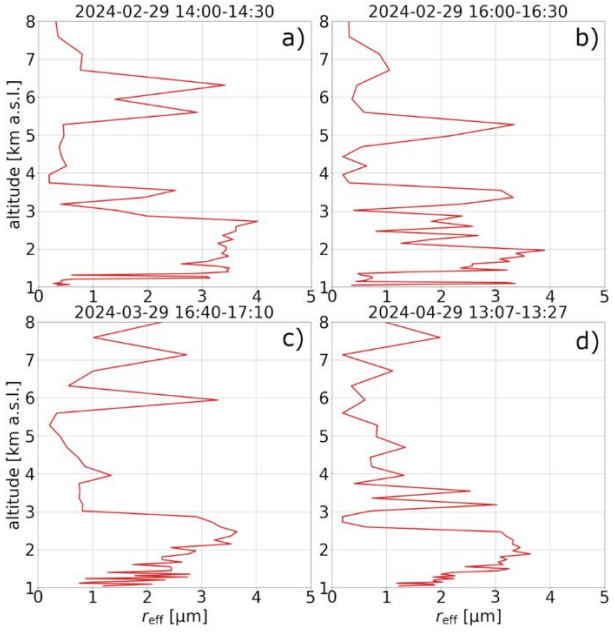

Figure 8: Profiles of effective radius of aerosol particles taken at (a, b) 29 February 2024, (c) 29 March 2024, and (d) 29 April 2024.

Examples of averaged r_{eff} profiles retrieved using APSD software are shown in Fig. 8. In the first two cases from 29 February 2024 (14 UTC and 16 UTC), the value of the effective radius up to 4 km reaches 3-4 µm, the second layer with approx. max. 3 µm is present between 5 and 6 km. The third example from 29 March 2024 shows the presence of a layer with particles of effective radius up to 3.5 µm reaching an altitude of 3 km. From 5.5 km up to 8 km, several aerosol layers are present with

https://doi.org/10.5194/egusphere-2026-1060
Preprint. Discussion started: 24 June 2026

particles r_{eff} up to 2 μm. Fourth example from 29 April 2024 shows a layer of higher values of r_{eff} present up to 3 km, and the second layer at about 3.5 km, where the values of r_{eff} are between 2.5 and 3 μm. In all cases, the size of particles of the "background" aerosol load is around 0.2-0.3 μm.

Fig. 9 presents the temporal evolution of the effective radius retrieved from the Cimel sun photometer located at Zugspitze. The successful retrieval was possible on 29 February 2024 between 7:37 and 14:39 UTC and on 29 April 2024 between 13:23 and 16:31 UTC. The figure shows the effective radii of the fine and coarse aerosol modes.

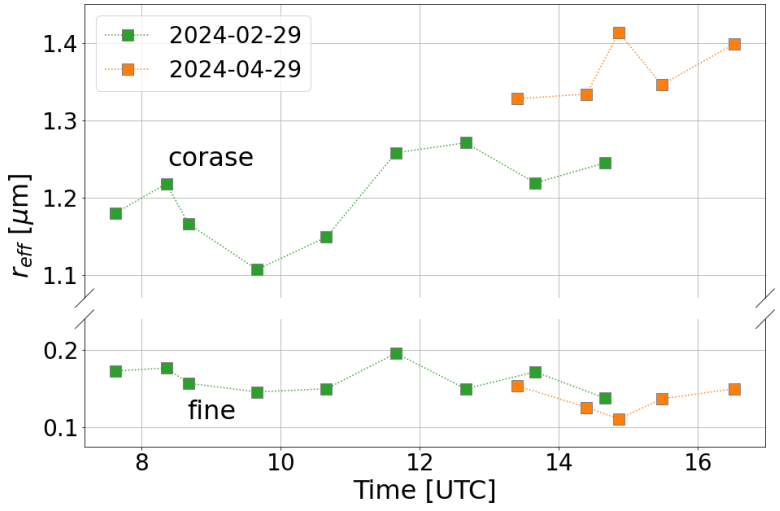

Figure 9: Diurnal variation of the effective radius retrieved from the AERONET Cimel sun photometer at Zugspitze on 29 February 2024 (green) and 29 April 2024 (orange). Circles and diamonds represent the effective radii of the coarse and fine aerosol modes, respectively.

On both days, the effective radius of fine particles varies from 0.1 to 0.2 μm, but the effective radius of coarse particles changes from 1.1 to 1.3 μm on 29 February 2024 and from 1.2 to over 1.4 μm on 29 April 2024.

The larger values (up to 3–4 μm) observed locally within individual dust layers should not be directly compared with the column-integrated AERONET product, which represents an optical average over the entire atmospheric column above the photometer. To compare the range-resolved lidar retrievals with the column-integrated AERONET product, an optically weighted effective radius was calculated from the lidar-derived profiles. The vertically resolved effective radius was weighted by the aerosol extinction coefficient profile:

$$r_{eff\,\alpha} = \frac{\int r_{eff}(z)\alpha(z)dz}{\int \alpha(z)dz}, \quad (12)$$

where $r_{eff}(z)$ is the lidar-derived effective radius profile and $\alpha(z)$ is the aerosol extinction coefficient profile. This approach assigns greater weight to aerosol layers contributing most strongly to the atmospheric optical depth and therefore provides a more meaningful comparison with the column-integrated sun-photometer retrievals. Since the AERONET sun photometer is

https://doi.org/10.5194/egusphere-2026-1060
Preprint. Discussion started: 24 June 2026

located at the summit of Zugspitze (2962 m a.s.l.), whereas the lidar is operated in Garmisch-Partenkirchen (734 m a.s.l.), only the part of the lidar profile above the altitude of the photometer was considered in the integration.

The aerosol extinction coefficient profile was retrieved from the 532 nm elastic backscatter signal using the Klett–Fernald inversion (Klett, 1985; Speidel and Vogelmann, 2023). A constant lidar ratio of 50 sr was assumed, which is representative of transported Saharan dust observed over Europe (Tesche et al., 2009; Freudenthaler et al., 2009).

The resulting optically weighted effective radii were 1.1 µm for 29 February 2024 and 1.4 µm for 29 April 2024 in good agreement with the AERONET coarse-mode effective radii of approximately 1.1–1.3 µm and 1.2–1.4 µm, respectively. For 29 March 2024, the optically weighted lidar-derived effective radius was 0.9 µm; however, no AERONET retrieval was available because of cloud cover.

4 Conclusions

This study presents detailed observations of Saharan dust intrusions over the Bavarian Alps during three events in February, March, and April 2024. The unique geographical setup of the Garmisch-Partenkirchen (Loisach valley) and the summit of Zugspitze, coupled with advanced ground-based remote sensing instrumentation (including a multi-wavelength lidar system and a Cimel sun photometer), enabled comprehensive characterization of the vertical distribution and microphysical properties of mineral dust transported over the Alps towards Central Europe.

Synoptic analyses revealed that each event was driven by distinct meteorological patterns enabling northward dust advection from North Africa. Despite differences in cloud cover and transport speed, all three cases showed clear evidence of elevated dust layers extending up to 6–7 km altitude, with multiple stratified layers identified particularly on 29 February and 29 April. On 29 March, although hindered by cloud cover, the rapid long-range transport of dust was inferred from HYSPLIT trajectory modelling and elevated model-predicted AODs. The dust layers observed with lidar could clearly be assigned to rapid long-range transport of dust from the Sahara. This was supported by HYSPLIT trajectory modelling and elevated model-predicted AODs.

Aerosol optical depth (AOD) and Ångström exponent (AE) measurements indicated a dominance of coarse-mode particles during dust episodes, with decreasing AE values corresponding to increased dust loading. Effective radius profiles retrieved using an inversion algorithm applied to multi-wavelength lidar signals consistently showed large particle sizes (up to 3–4 µm) within elevated dust layers. To enable a direct comparison with the column-integrated AERONET product, an optically weighted effective radius was calculated from the lidar-derived profiles. The resulting values of 1.1 µm (29 February 2024) and 1.4 µm (29 April 2024) were in good agreement with the coarse-mode effective radii retrieved from the Zugspitze sun photometer (approximately 1.2–1.4 µm). Vertical profiles of effective radius further confirmed the presence of well-defined dust layers with particle sizes generally decreasing with altitude. The observed single scattering albedo (SSA) values, particularly on 29 April, were characteristic of pure mineral dust. In contrast, those on 29 February suggested a mixture of mineral dust and anthropogenic aerosols, presumably from residential wood-burning emissions.

https://doi.org/10.5194/egusphere-2026-1060
Preprint. Discussion started: 24 June 2026

The use of the APSD inversion software, incorporating a bimodal log-normal distribution and Mie theory, proved effective in deriving detailed microphysical parameters of the aerosol plumes. The synergy between lidar and photometric observations significantly enhanced the reliability of aerosol classification and quantification. The results underline the value of high-resolution, range-resolved remote sensing data in identifying the structure and evolution of aerosol layers, especially in complex mountainous terrain.

In summary, these observations provide compelling evidence for the frequent and significant impact of Saharan dust on atmospheric composition over Central Europe, even outside the Mediterranean basin. The findings contribute to the understanding of dust transport dynamics, vertical distribution, and radiative properties in the mid-latitudes. Continued monitoring using integrated remote sensing platforms is essential for improving dust forecasting, assessing its climatic impacts, and quantifying aerosol-radiation-cloud interactions in regional climate models.

Data availability

AERONET observations are publicly available from the NASA AERONET database. The lidar measurements and retrieval products used in this study are available through the ACTRIS/EARLINET data portal. The specific dataset used to generate the figures and results presented in this paper will also be archived in the Zenodo repository and assigned a DOI upon acceptance of the manuscript.

Author contributions

MP: conceptualization, formal analysis, data curation, investigation, visualization, writing – original draft and writing – review and editing, JS: writing – original draft and writing – review and editing, SS: methodology and software, TS: conceptualization, methodology, software and writing – original draft, HV: project administration, supervision, writing – original draft and writing – review and editing.

Competing interests

The contact author has declared that none of the authors has any competing interests.

Disclaimer

Copernicus Publications remains neutral about jurisdictional claims made in the text, published maps, institutional affiliations, or any other geographical representation in this paper. While Copernicus Publications makes every effort to include appropriate place names, the final responsibility lies with the authors. Views expressed in the text are those of the authors and do not necessarily reflect the views of the publisher.

https://doi.org/10.5194/egusphere-2026-1060
Preprint. Discussion started: 24 June 2026

Acknowledgements

ACTRIS Germany (ACTRIS-D) is acknowledged for funding the equipment used in this study. We further acknowledge the ACTRIS Calibration and Data Services (CARS) for supporting lidar calibration and quality assurance activities. AERONET-Europe, part of the ACTRIS Research Infrastructure, is acknowledged for providing calibration services. We acknowledge the NOAA Air Resources Laboratory (ARL) for the provision of the HYSPLIT transport and dispersion model and the READY website (https://www.ready.noaa.gov) used in this publication. We further acknowledge the Copernicus Atmosphere Monitoring Service (CAMS) and the CAMS Atmosphere Data Store for providing CAMS aerosol data.

Financial support

This work was funded by the German Federal Ministry of Research, Technology, and Space (BMFTR) within the ACTRIS-D project (grant no. 01LK2001B) and by the Helmholtz Research Program Changing Earth – Sustaining our Future within the Helmholtz research field Earth and Environment. Open access to this publication was made possible by the Karlsruhe Institute of Technology (KIT).

Review statement

The review statement will be added by Copernicus Publications, listing the handling editor as well as all contributing referees according to their status, anonymous or identified.

References

Ansmann, A., Bösenberg, J., Chiakovsky, A., Comerón, A., Eckhardt, S., Eixmann, R., Freudenthaler, V., Ginoux, P., Komguem, L., Linné, H., Lopez Marquez, M. Á., Matthias, V., Mattis, I., Mitev, V., Müller, D., Music, S., Nickovic, S., Pelon, J., Sauvage, L., Sobolewsky, P., Srivastava, M. K., Stohl, A., Torres, O., Vaughan, G., Wandinger, U., and Wiegner, M.: Long-range transport of Saharan dust to northern Europe: The 11-16 October 2001 outbreak observed with EARLINET Journal of Geophysical Research, 108 (D24), 0148-0227, http://doi.org/10.1029/2003jd003757, 2003.

Balis, D. S., Amiridis, V., Nickovic, S., Papayannis, A., and Zerefos, C.: Optical properties of Saharan dust layers as detected by a Raman lidar at Thessaloniki, Greece Geophysical Research Letters, 31 (13), L13104 1-4, http://doi.org/10.1029/2004GL019881, 2004.

Bi, L., Lin, W., Wang, Z., Tang, X., Zhang, X., and Yi, B.: Optical Modeling of Sea Salt Aerosols: The Effects of Nonsphericity and Inhomogeneity, Journal of Geophysical Research: Atmospheres, 123 (1), 543 – 558, https://doi.org/10.1002/2017JD027869, 2018.

https://doi.org/10.5194/egusphere-2026-1060
Preprint. Discussion started: 24 June 2026

Bohren, C. F., and Huffman, D. R.: Absorption and Scattering of Light by Small Particles, John Wiley & Sons, New York, 1999.

Böckmann, C.: Hybrid regularization method for the ill-posed inversion of multiwavelength lidar data in the retrieval of aerosol size distributions, Applied Optics, 40 (9), pp. 1329–1342, https://doi.org/10.1364/AO.40.001329, 2001.

Böckmann, C., Ritter, C., and Graßl, S.: Improvement of Aerosol Coarse-Mode Detection through Additional Use of Infrared Wavelengths in the Inversion of Arctic Lidar Data, Remote Sensing, 16 (9), 1576, https://doi.org/10.3390/rs16091576, 2024.

Carslaw, K. S., Boucher, O., Spracklen, D. V., Mann, G. W., Rae, J. G. L., Woodward, S., and Kulmala, M.: A review of natural aerosol interactions and feedbacks within the Earth system, Atmospheric Chemistry and Physics, 10, 1701–1737, https://doi.org/10.5194/acp-10-1701-2010, 2010.

Devara, P. C. S.: Review article Remote sensing of atmospheric aerosols from active and passive optical techniques, International Journal of Remote Sensing, 19 (17), 3271–3288, http://doi.org/10.1080/014311698213966, 1998.

Dubovik, O., Sinyuk, A., Lapyonok, T., Holben, B. N., Mishchenko, M., Yang, P., Eck, T. F., Volten, H., Muñoz, O., Veihelmann, B., van der Zande, W. J., Leon, J.-F., Sorokin, M., and Slutsker, I.: Application of spheroid models to account for aerosol particle nonsphericity in remote sensing of desert dust, Journal of Geophysical Research Atmospheres, 111 (11), D11208, http://doi.org/10.1029/2005JD006619, 2006.

Dubovik, O., Fuertes, D., Litvinov, P., Lopatin, A., Lapyonok, T., Doubovik, I., Xu, F., Ducos, F., Chen, C., Torres, B., Derimian, Y., Li, L., Herreras-Giralda, M., Herrera, M., Karol, Y., Matar, C., Schuster, G. L., Espinosa, R., Puthukkudy, A., Li, Z., Fischer, J., Preusker, R., Cuesta, J., Kreuter, A., Cede, A., Aspetsberger, M., Marth, D., Bindreiter, L., Hangler, A., Lanzinger, V., Holter, C., and Federspiel, C.: A Comprehensive Description of Multi-Term LSM for Applying Multiple a Priori Constraints in Problems of Atmospheric Remote Sensing: GRASP Algorithm, Concept, and Applications, Frontiers in Remote Sensing, 2, 706851, http://doi.org/10.3389/frsen.2021.706851, 2021.

Freudenthaler, V., Esselborn, M., Wiegner, M., Pisani, G., Ansmann, A., Müller, D., Tesche, M., Engelmann, R., Althausen, D., Groß, S., and Pappalardo, G.: Depolarization ratio profiling at several wavelengths in pure Saharan dust during SAMUM 2006, Tellus B: Chemical and Physical Meteorology, 61 (1), 165–179, https://doi.org/10.1111/j.1600-0889.2008.00396.x, 2009.

Freudenthaler, V.: About the effects of polarising optics on lidar signals and the Δ90 calibration, Atmospheric Measurement Techniques, 9, 4181–4255, https://doi.org/10.5194/amt-9-4181-2016, 2016.

Freudenthaler, V., Linné, H., Chaikovski, A., Rabus, D., and Groß, S.: EARLINET lidar quality assurance tools, Atmospheric Measurement Techniques Discussions, https://doi.org/10.5194/amt-2017-395, 2018.

Giles, D. M., Sinyuk, A., Sorokin, M. G., Schafer, J. S., Smirnov, A., Slutsker, I., Eck, T. F., Holben, B. N., Lewis, J. R., Campbell, J. R., Welton, E. J., Korkin, S. V., and Lyapustin, A. I.: Advancements in the Aerosol Robotic Network (AERONET) Version 3 database – automated near-real-time quality control algorithm with improved cloud screening for Sun photometer aerosol optical depth (AOD) measurements, Atmospheric Measurement Techniques, 12, 169–209, https://doi.org/10.5194/amt-12-169-2019, 2019.

https://doi.org/10.5194/egusphere-2026-1060
Preprint. Discussion started: 24 June 2026

Groß, S., Freudenthaler, V., Toledano, C., Schäfler, A., and Wiegner, M.: Characterization of Saharan dust, biomass-burning smoke and mixtures of biomass-burning smoke and dust by means of multi-wavelength depolarization and Raman lidar measurements during SAMUM 2, Tellus B: Chemical and Physical Meteorology, 63 (4), 706–724, https://doi.org/10.1111/j.1600-0889.2011.00556.x, 2011.

Hoshyaripour, G. A., Bachmann, V., Förstner, J., Steiner, A., Vogel, H., Wagner, F., Walter, C., and Vogel, B.: Effects of Particle Nonsphericity on Dust Optical Properties in a Forecast System: Implications for Model-Observation Comparison, Journal of Geophysical Research: Atmospheres, 124 (13), 7164 – 7178, https://doi.org/10.1029/2018JD030228, 2019.

Huang, Y., Kok, J. F., Saito, M., and Muñoz, O.: Single-scattering properties of ellipsoidal dust aerosols constrained by measured dust shape distributions, Atmospheric Chemistry and Physics, 23 (4), 2557 – 2577, https://doi.org/10.5194/acp-23-2557-2023, 2023.

Inness, A., Ades, M., Agustí-Panareda, A., Barr, J., Benedictow, A., Blechschmidt, A.-M., Jose Dominguez, J., Engelen, R., Eskes, H., Flemming, J., Huijnen, V., Jones, L., Kipling, Z., Massart, S., Parrington, M., Peuch, V.-H., Razinger, M., Remy, S., Schulz, and M., Suttie, M.: The CAMS reanalysis of atmospheric composition, Atmospheric Chemistry and Physics, 19 (6), 3515–3556, https://doi.org/10.5194/acp-19-3515-2019, 2019.

Jäger, H., Carnuth, W., and Georgi, B.: Observations of Saharan Dust at a North Alpine Station, Journal of Aerosol Science, 19, 1235–1238, https://doi.org/10.1016/0021-8502(88)90144-9, 1988.

Jagodnicka, A. K., Stacewicz, T., Karasinski, G., Posyniak, M., and Malinowski, S. P.: Particle size distribution retrieval from multiwavelength lidar signals for droplet aerosol, Applied Optics 48, B8–B16, https://doi.org/10.1364/AO.48.0000B8, 2009.

Laj, P., Myhre, C., L., Riffault, V., Amiridis, V., Fuchs, H., Eleftheriadis, K., Petäjä, T., Salameh, T., Kivekäs, N., Juurola, E., Saponaro, G., Philippin, S., Cornacchia, C., Arboledas, L., A., Baars, H., Claude, A., De, Mazière, M., Dils, B., Dufresne, M., Evangeliou, N., Favez, O., Fiebig, M., Haeffelin, M., Herrmann, H., Höhler, K., Illmann, N., Kreuter, A., Ludewig, E., Marinou, E., Möhler, O., Mona, L., Murberg, L.E., Nicolae, D., Novelli, A., O'Connor, E., Ohneiser, K., Altieri, R., M., P., Picquet-Varrault, B., van, Pinxteren, D., Pospichal, B., Putaud, J.-P., Reimann, S., Siomos, N., Stachlewska, I., Tillmann, R., Voudouri, K.A., Wandinger, U., Wiedensohler, A., Apituley, A., Comerón, A., Gysel-Beer, M., Mihalopoulos, N., Nikolova, N., Pietruczuk, A., Sauvage, S., Sciare, J., Skov, H., Svendby, T., Swietlicki, E., Tonev, D., Vaughan, G., Zdimal, V., Baltensperger, U., Doussin, J.-F., Kulmala, M., Pappalardo, G., Sundet, S.S., and Vana, M.: Aerosol, Clouds and Trace Gases Research Infrastructure (ACTRIS): The European Research Infrastructure Supporting Atmospheric Science, Bulletin of the American Meteorological Society, 105 (7), E1098–E1136, https://doi.org/10.1175/BAMS-D-23-0064.1, 2024.

Liu, Y., Jia, R., Dai, T., Xie, Y., and Shi, G.: A review of aerosol optical properties and radiative effects, Journal of Meteorological Research, 28 (6), 1003–1028, https://doi.org/10.1007/s13351-014-4045-z, 2014.

Lopatin, A., Dubovik, O., Fuertes, D., Stenchikov, G., Lapyonok, T., Veselovskii, I., Wienhold, F.G., Shevchenko, I., Hu, Q., and Parajuli, S.: Synergy processing of diverse ground-based remote sensing and in situ data using the GRASP algorithm: applications to radiometer, lidar, and radiosonde observations, Atmospheric Measurement Techniques, 14 (3), 2575–2614, https://doi.org/10.5194/amt-14-2575-2021, 2021.

https://doi.org/10.5194/egusphere-2026-1060
Preprint. Discussion started: 24 June 2026

Makuch, P., Sitarek, S., Markuszewski, P., Petelski, T., and Stacewicz, T.: Lidar observation of aerosol transformation in the atmospheric boundary layer above the Baltic Sea, Oceanologia, 63 (2), 238–246, https://doi.org/10.1016/j.oceano.2021.01.002, 2021.

Mylonaki, M., Giannakaki, E., Papayannis, A., Papanikolaou, C.-A., Komppula, M., Nicolae, D., Papagiannopoulos, N., Amodeo, A., Baars, H., and Soupiona, O.: Aerosol type classification analysis using EARLINET multiwavelength and depolarization lidar observations, Atmospheric Chemistry and Physics, 21 (3), 2211–2227, https://doi.org/10.5194/acp-21-2211-2021, 2021.

Papanikolaou, C.-A., Papayannis, A., Gidarakou, M., Abdullaev, S. F., Ajtai, N., Baars, H., Balis, D., Bortoli, D., Bravo-Aranda, J.A., Collaud-Coen, M., de, Rosa, B., Dionisi, D., Eleftheratos, K., Engelmann, R., Floutsi, A. A., Abril-Gago, J., Goloub, P., Giuliano, G., Gumà-Claramunt, P., Hofer, J., Hu, Q., Komppula, M., Marinou, E., Martucci, G., Mattis, I., Michailidis, K., Muñoz-Porcar, C., Mylonaki, M., Mytilinaios, M., Nicolae, D., Rodríguez-Gómez, A., Salgueiro, V., Shang, X., Stachlewska, I. S., Ștefănie, H. I., Szczepanik, D. M., Trickl, T., Vogelmann, H., and Voudouri, K. A.: Large-Scale Network-Based Observations of a Saharan Dust Event across the European Continent in Spring 2022, Remote Sensing, 16 (17), 3350, https://doi.org/10.3390/rs16173350, 2024.

Papayannis, A., Balis, D., Amiridis, V., Chourdakis, G., Tsaknakis, G., Zerefos, C., Castanho, A. D. A., Nickovic, S., Kazadzis, S., and Grabowski, J.: Measurements of Saharan dust aerosols over the eastern Mediterranean using elastic backscatter-Raman lidar, spectrophotometric and satellite observations in the frame of the EARLINET project, Atmospheric Chemistry and Physics, 5 (8), 2065–2079, http://doi.org/10.5194/acp-5-2065-2005, 2005.

Papayannis, A., Amiridis, V., Mona, L., Tsaknakis, G., Balis, D., Bösenberg, J., Chaikovski, A., De, Tomasi, F., Grigorov, I., Mattis, I., Mitev, V., Müller, D., Nickovic, S., Pérez, C., Pietruczuk, A., Pisani, G., Ravetta, F., Rizi, V., Sicard, M., Trickl, T., Wiegner, M., Gerding, M., Mamouri, R.E., D'Amico, G., and Pappalardo, G.: Systematic lidar observations of Saharan dust over Europe in the frame of EARLINET (2000-2002), Journal of Geophysical Research Atmospheres, 113 (10), D10204, https://doi.org/10.1029/2007JD009028, 2008.

Pappalardo, G., Amodeo, A., Apituley, A., Comeron, A., Freudenthaler, V., Linné H., Ansmann, A., Bösenberg, J., D'Amico, G., Mattis, I., Mona, L., Wandinger, U., Amiridis, V., Alados-Arboledas, L., Nicolae, D., and Wiegner, M.: EARLINET: towards an advanced sustainable European aerosol lidar network, Atmospheric Measurement Techniques, 7 (8), 2389–2409, https://doi.org/10.5194/amt-7-2389-2014, 2014.

Pappalardo, G.: ACTRIS Aerosol, Clouds and Trace Gases Research Infrastructure, EPJ Web of Conferences, 176, 09004, https://doi.org/10.1051/epjconf/201817609004, 2018.

Rolph, G., Stein, A., and Stunder, B.: Real-time Environmental Applications and Display sYstem: READY. Environmental Modelling & Software, 95, 210–228, https://doi.org/10.1016/j.envsoft.2017.06.025, 2017.

Seinfeld, J. H., and Pandis, S. N.: Atmospheric Chemistry and Physics, John Wiley & Sons, New York, 1997.

Seinfeld, J., H., Bretherton, C., Carslaw, K., S., Coe, H., DeMott, P., J., Dunlea, E., J., Feingold, G., Ghan, S., Guenther, A., B., Kahn, R., Kraucunas, I., Kreidenweis, S., M., Molina, M., J., Nenes, A., Penner, J., E., Prather, K., A., Ramanathan, V.,

https://doi.org/10.5194/egusphere-2026-1060
Preprint. Discussion started: 24 June 2026

Ramaswamy, V., Rasch, P., J., Ravishankara, A., R., Rosenfeld, D., Stephens, G., and Wood, R.: Improving our fundamental understanding of the role of aerosol-cloud interactions in the climate system, Proceedings of the National Academy of Sciences of the United States of America, 113 (21), 5781-5790, https://doi.org/10.1073/pnas.1514043113, 2016.

Sicard, M., D'Amico, G., Comerón, A., Mona, L., Alados-Arboledas, L., Amodeo, A., Baars, H., Baldasano, J.M., Belegante, L., Binietoglou, I., Bravo-Aranda, J.A., Fernández, A.J., Fréville, P., García-Vizcaíno, D., Giunta, A., and Granados-Muñoz, M. J.: EARLINET: Potential operationality of a research network, Atmospheric Measurement Techniques, 8 (11), 4587 – 4613, https://doi.org/10.5194/amt-8-4587-2015, 2015.

Sitarek, S., Stacewicz, T., and Posyniak, M.: Software for retrieval of aerosol particle size distribution from multiwavelength lidar signals, Computer Physics Communications 199, 53-60, https://doi.org/10.1016/j.cpc.2015.08.024, 2016.

Shin, S.-K., Tesche, M., Noh, Y., and Müller, D.: Aerosol-type classification based on AERONET version 3 inversion products, Atmospheric Measurement Techniques, 12 (7), 3789–3803, https://doi.org/10.5194/amt-12-3789-2019, 2019.

Speidel, J., and Vogelmann, H.: Correct(ed) Klett–Fernald algorithm for elastic aerosol backscatter retrievals: a sensitivity analysis, Applied Optics, 62 (4), 861-868, https://doi:10.1364/AO.465944, 2023.

Stacewicz, T., Posyniak, M., Sitarek, S., and Malinowski, S.P.: Lidar retrievals of cloud droplet number concentration at the cumulus base: A feasibility study, Atmospheric Research, 142, 32–39, https://doi.org/10.1016/j.atmosres.2013.10.023, 2014.

Stein, A. F., Draxler, R. R., Rolph, G. D., Stunder, B. J. B., Cohen, M. D., and Ngan, F.: NOAA's HYSPLIT atmospheric transport and dispersion modeling system, Bulletin of the American Meteorological Society, 96 (12), 2059 – 2077, http://doi.org/10.1175/BAMS-D-14-00110.1, 2015.

Tesche, M., Ansmann, A., Müller, D., Althausen, D., Mattis, I., Heese, B., Freudenthaler, V., and Wiegner, M.: Vertical profiling of Saharan dust with Raman lidars and airborne HSRL in southern Morocco during SAMUM, Tellus B: Chemical and Physical Meteorology, 61 (1), 144–164, https://doi.org/10.1111/j.1600-0889.2008.00390.x, 2009.

Trickl T., Vogelmann, H., Ries, L., and Sprenger, M.: Very high stratospheric influence observed in the free troposphere over the northern Alps — just a local phenomenon?, Atmospheric Chemistry and Physics, 20, 243–266, http://doi.org/10.5194/acp-20-243-2020, 2020.

Trickl, T., Vogelmann, H., Fromm, M. D., Jäger, H., and Perfahl, M., Steinbrecht W.: Measurement report: Violent biomass burning and volcanic eruptions - a new period of elevated stratospheric aerosol over central Europe (2017 to 2023) in a long series of observations, Atmospheric Chemistry and Physics, 24 (3), 1997–2021, https://doi.org/10.5194/acp-24-1997-2024, 2024.

Vogelmann, H., Sussmann, R., Trickl, T., and Reichert, A.: Spatiotemporal variability of water vapor investigated using lidar and FTIR vertical soundings above the Zugspitze, Atmospheric Chemistry and Physics, 15, 3135-3148, https://doi.org/10.5194/acp-15-3135-2015, 2015.

Xian, P., Reid, J. S., Hyer, E. J., Sampson, C. R., Rubin, J. I., Ades, M., Asencio, N., Basart, S., Benedetti, A., Bhattacharjee, P. S., Brooks, M. E., Colarco, P. R., da, Silva, A. M., Eck, T. F., Guth, J., Jorba, O., Kouznetsov, R., Kipling, Z., Sofiev, M., Perez, Garcia-Pando, C., Pradhan, Y., Tanaka, T., Wang, J., Westphal, D. L., Yumimoto, K., and Zhang, J.: Current state of

https://doi.org/10.5194/egusphere-2026-1060
Preprint. Discussion started: 24 June 2026

the global operational aerosol multi-model ensemble: An update from the International Cooperative for Aerosol Prediction (ICAP), Quarterly Journal of the Royal Meteorological Society, 145 (S1), 176–209, https://doi.org/10.1002/qj.3497, 2019.

Zhang B.: The Effect of Aerosols to Climate Change and Society, Journal of Geoscience and Environment Protection, 8, 55-78, https://doi.org/10.4236/gep.2020.88006, 2020.